Proceedings 5th African Rift geothermal Conference
Arusha, Tanzania, 29-31 October 2014

Cost-effective aerial imagery and soil CO_2 flux surveys for geothermal exploration

Kenneth B. (Keg) Alexander[1] and Mark Harvey[2]

IESE – Auckland UniServices[1], School of Environment[2]

The University of Auckland, New Zealand

Keg.alexander@gmail.com; mharvey098@aucklanduni.ac.nz

Keywords: orthophotos, digital surface models, soil CO_2 flux surveys

ABSTRACT

Soil CO_2 flux surveys offer a relatively new approach to evaluate volcanic and geothermal areas that can provide detailed information relating to a system's characteristics, including geology, hydrology, geochemistry, and heat flow. CO_2 flux may indicate where degassing geothermal fluids are present in the near subsurface and their upflow is enhanced by permeable structures such as faults. After water, CO_2 is the principal component of typical geothermal gases, and is easily detectable. Accordingly, it is the most appropriate component to focus on during geothermal exploration.

Standard preparations for a soil CO_2 survey include identification of possible fault traces on the ground surface using remote sensing techniques such as aerial photographs (orthophotos) or LiDAR. High resolution (<0.1 m) imagery and data are typically collected by sensors mounted on board manned light aircraft. Lower resolution imagery (>0.5 m) can be obtained from satellite. ~~The imagery is used to identify possible lineaments and fault traces.~~ Then, CO_2 flux measurements can be collected by transecting the identified faults, or in a grid pattern around fault intersections.

A rapidly advancing alternative for collection of aerial imagery utilises ~~is the collection of imagery from~~ sensors mounted on unmanned aerial vehicles (UAVs). Such imagery can be used to produce high resolution (<0.1 m) orthophotos, or digital surface model (DSMs) of comparable quality to LiDAR. UAVs can produce orthophotos and DSMs at a fraction of the cost of manned aircraft and at a higher resolution than is currently available from satellite.

In this paper, we suggest a cost-efficient approach for geothermal exploration in arid areas (such as the East African Rift), which combines DSM mapping by UAVs, geological evaluation of structural features, and focused soil CO_2 flux surveys to identify potential permeable faults, and by extension, exploration well targets. Examples of results of recent UAV aerial imagery and CO_2 flux surveys are provided.

1. INTRODUCTION

Possible fault locations on the ground surface are commonly mapped using aerial photographs, satellite imagery, or, more recently, digital surface models (DSMs) and digital elevation models (DEMs). A DSM is a virtual representation of the earth's surface and includes all objects on it, such as vegetation and buildings; A DEM is a representation of the earth's bare surface without vegetation or buildings (Priestnall et al., 2000). High resolution (<0.1 m) DSMs and DEMs are typically collected by sensors mounted on board manned light aircraft. Lower resolution imagery (>0.5 m) can be obtained from satellite (Lejot et al., 2007). Sensors can include Light Detection and Ranging (LiDAR), digital cameras (photogrammetry), or infrared.

Photogrammetry is a technology that allows measurements to be made from photographs and, for the reconstruction of three dimensional information (i.e. DSM), from a mosaic of overlapping, two dimensional photographs (Li et al., 2010). Although photogrammetry is not a new technology, recent advances in unmanned aerial vehicles (UAV) equipped with global positioning systems (GPS) and digital cameras have reduced the cost of collecting imagery. Modern desktop and cloud computing power allows for routine post processing of large numbers of individual images. The individual photos are combined into aerial orthophotos and DSMs of comparable quality (<0.1 m) to airborne LiDAR (Harwin & Lucieer, 2012; Fonstad et al., 2013).

High quality aerial photos (orthophotos) and DSMs are useful for all phases of geothermal exploration and development. Examples include maps for geological, geochemical, and geophysical surveys (van der Meer et al., 2014), environmental baseline studies, geotechnical studies, civil works, steam field design, and plant design and construction (Li et al., 2010). Typically, geologists use orthophotos or DSMs to evaluate surface structural features and map potential fault locations.

Soil CO_2 flux surveys are usually undertaken to determine if areas of elevated CO_2 flux and/or elevated shallow (≤1 m) subsurface temperature support the presence of mapped faults, and to identify other potential structural features that may be providing anomalous temperature and gas flux. Elevated CO_2 flux may indicate areas where degassing geothermal fluids are present in the subsurface~~, and their upflow is focused on permeable structures.~~

Historically, CO_2 surveys were performed to measure soil gas CO_2 ***concentration*** in the soil (% of CO_2 relative to other gases). Instead, it is more useful to perform soil CO_2 ***flux*** surveys that measure the CO_2 flux – that is, the mass of CO_2 (grams) flowing through a given cross-sectional area of soil (m^2) per unit of time (day). The flux technique has superseded static concentration surveys because it offers the following advantages:

- Provides a direct measurement of the CO_2 flux out of the soil, which may indicate degassing through a permeable structure such as a fault
- Provides immediate results allowing survey coverage to be adapted in real time
- Faster (roughly ~~50~~ 40 measurements/day depending on conditions)
- Biological (background) CO_2 flux can be identified and separated from geothermal~~ly sourced~~ flux
- Can ~~possibly~~ be used to estimate heat flow (can provide MWth estimate for the area if the ~~deep fluid~~ CO_2:H2O ratio of the steam phase supplying the thermal area ~~concentration and enthalpy~~ is known)
- Can be used to establish an environmental baseline for CO_2 emissions prior to development

Commented [MH1]: 40 is more realistic as the time for a single measurement is now about 240seconds (used to be about 90s)

In this paper, we describe a cost-effective geothermal prospecting tool by combining aerial imagery and soil CO_2 flux surveys to identify possible permeable faults. As examples, we provide case studies of a recent UAV-derived DSM produced from aerial images of the Poihipi geothermal steam field in New Zealand (Harvey et al., 2014) and a soil CO_2 flux survey at the San Jacinto-Tizate geothermal power project in Nicaragua (Harvey et al, 2011).

2. METHODOLOGY

2.1 Aerial imagery

For the Poihipi survey (Harvey et al, 2014), aerial imagery was collected using a modified DJI Phantom 2 Vision+ quadcopter (Figure 1). The quadcopter was modified by the replacement of the stock camera with a Canon A2400 camera (16MP); the stock camera has a wide-angle (fish-eye) lens that is not ideal for photogrammetry. The Canon camera was programmed to autonomously capture images (5 second intervals) during flight.

Figure 1: DJI Phantom Vision 2+ quadcopter (Harvey et al., 2014)

Formatted: Font: Bold

An appropriate flight plan was determined using DJI Ground Station® software. The flight plan was then uploaded to the quadcopter's flight controller using the DJI Vision App. Both in-flight navigation and image capture were autonomous.

Ground control points (GCP) were established prior to flight by placing yellow duct tape on established survey benchmarks. The survey benchmark locations were last checked in 2013 and the average elevation (Z) error was 3.8 mm. Most benchmarks were located on geothermal steam line footings, immediately adjacent to Poihipi Road, Taupo. Coordinates for 12 ground control points (GCPs) were utilized to georeference the resulting orthophoto and DEM.

Three flights were conducted, each of approximately 17 minutes duration giving a total flight time of about 50 minutes. Flight altitude was 120 m (relative to the launch point), with a ground speed of 4 m/s. More than 300 overlapping images were processed using Agisoft Photoscan®, commercial photogrammetry software (Figure 2).

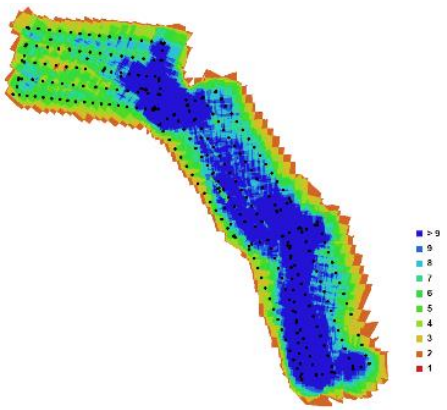

Figure 2: Camera image locations and overlap (numbers refer to number of images that capture that area) (Harvey et al., 2014).

2.2 Soil CO_2 flux

For the San Jacinto-Tizate survey (Harvey et al, 2011), structural features were evaluated using aerial photographs, DEMs, surface geological mapping, and drilling results. DEM images were imported into a 3D surface mapping program (Golden Software's Surfer®) and were evaluated by adjusting parameters such as lighting and sun angle. Several NNE-trending faults were identified including the Los Tablones Fault, which showed a clear offset of topography indicating vertical movement (Figure 3). Elevated CO_2 flux emanating from this fault would suggest a permeable fault and a possible pathway for geothermal fluids.

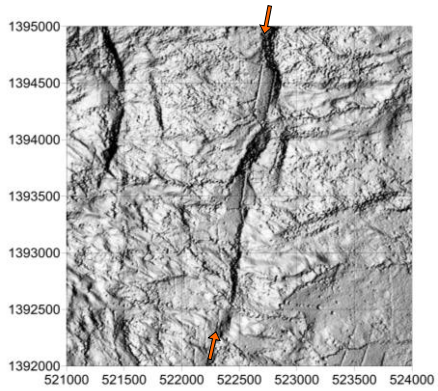

Figure 3: DEM from San Jacinto-Tizate survey showing the Los Tablones Fault (UTM WGS84).

A soil CO_2 flux survey was designed to intersect the Los Tablones Fault and other structures in the area. ~~along a dozen east-west transects.~~ More than 600 flux measurements were made along the transects at 25 to 100 m intervals using a West Systems portable soil gas flux meter (Figure 4). CO_2 flux is calculated by placing a 200-mm diameter accumulation chamber on the soil surface and pressing it into the soil to obtain a seal. Gases flowing into the chamber are pumped to an infrared gas analyser. The instrument records the increase in CO_2 concentration inside the chamber over time. The rate of concentration increase is proportional to flux.

Figure 4: Soil CO_2 flux measurement at San Jacinto, July 2011. CO_2 flux analyser is worn as a backpack, and accumulation chamber placed over soil (Harvey et al, 2011).

After measurements are made, post processing of the data is required. It is important to identify the biological background component of the CO_2 flux, so that it is not confused with the geothermal signal. This is particularly important in areas where the geothermal reservoir is known or suspected to have low gas content. For the San Jacinto-Tizate survey, background CO_2 flux was identified using the graphical statistical approach (GSA), which separates log-normally distributed populations using cumulative

probability plots (Chiodini et al., 1998; Fridriksson et al., 2006). Inflection points in cumulative probability plots can be used to distinguish the presence of multiple populations (Sinclair, 1974).

There is only one clear inflection point in Figure 5 (13 $g \cdot m^{-2} \cdot d^{-1}$) and this value probably represents the threshold between background biological CO_2 flux and geothermal flux at San Jacinto. This value is equal to the global mean background soil CO_2 flux for tropical environments (13 ± 6.8 $g \cdot m^{-2} \cdot d^{-1}$) (Bond-Lamberty & Thomson, 2010), which provides support to this argument.

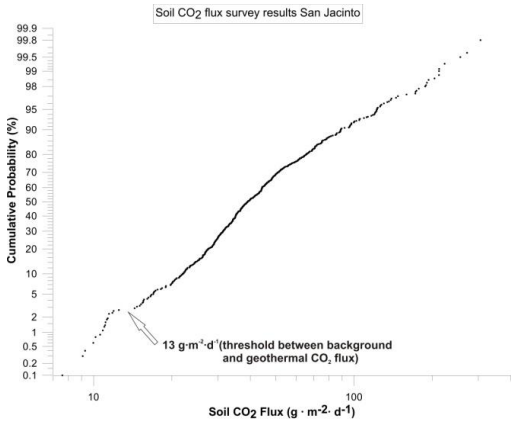

Figure 5: Cumulative probability plot for soil CO_2 flux measurements at San Jacinto-Tizate (Harvey et al, 2011).

3. RESULTS

3.1 Aerial imagery

For the Poihipi survey, image processing provided an orthophoto and DSM with 0.61 km^2 coverage area (Figure 6). Ground resolution was 3 cm (pixel size).

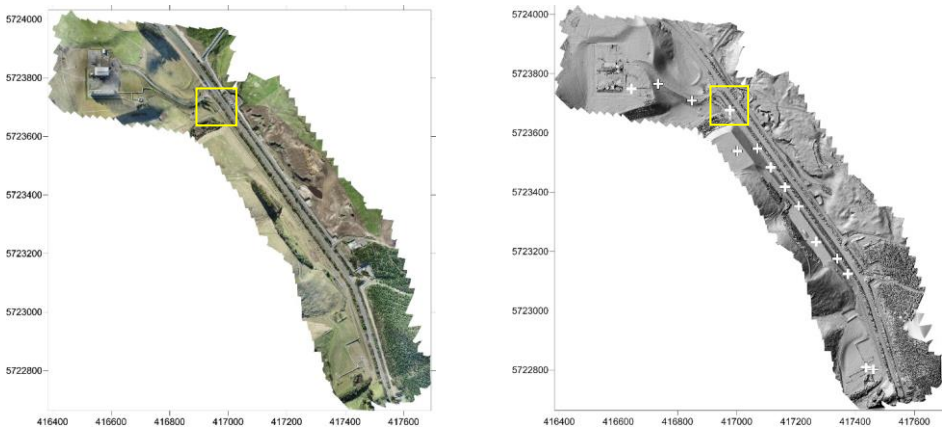

Figure 6: Orthophoto (on left) and Digital Surface Model (on right), Poihipi Road, Taupo, New Zealand (UTM WGS84). Yellow square shows detail area (Figure 7). Length of horizontal axis is approximately 1300 m (Harvey et al., 2014)**.**

Smaller areas have been expanded to show the quality of the imagery (Figure 7). The orthophoto and DSM have a ground resolution of 0.03 m pixel size, which is almost two orders of magnitude higher than LiDAR imagery (2 m pixel size) of the same area. The DSM images (Figure 5 and 6) show both the land surface, and buildings/vegetation covering the ground. It is possible to

produce DEMs with the data collected during the Poihipi Rd survey but this was not attempted (vegetation and buildings can be removed using tools within Agisoft Photoscan®).

Figure 7: Orthophoto (on left) and Digital Surface Model (on right), Poihipi Road, Taupo, New Zealand (UTM WGS84). Yellow square shows detail area (Figure 8). Length of horizontal axis is approximately 200 m (Harvey et al., 2014).

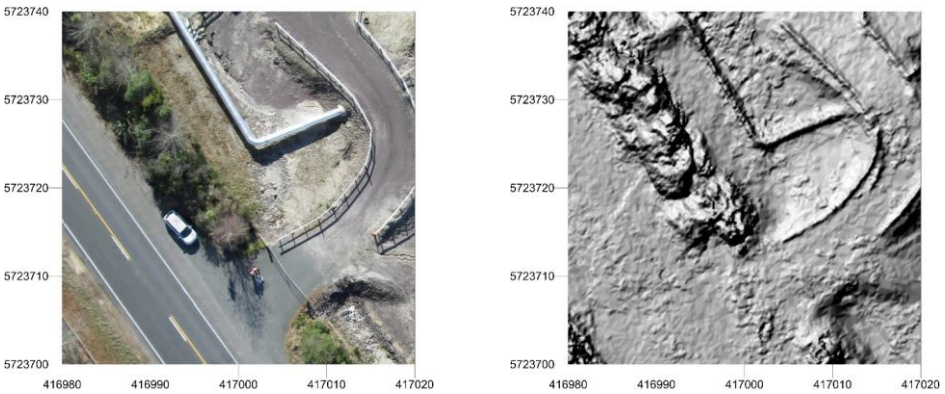

Figure 8: Fine detail orthophoto (on left) and DSM (on right), Poihipi Road, Taupo, New Zealand (UTM WGS84). Length of horizontal axis is approximately 40 m (Harvey et al., 2014).

3.2 Soil CO_2 flux

Soil CO_2 flux results are shown as point data in Figure 9. For clarity, only two levels (80 and 100 $g \cdot m^{-2} \cdot d^{-1}$) are used to classify the strength of the anomaly based on the measured gas flux at each measurement location.

The presence of strong soil CO_2 flux anomalies nearby to San Jacinto village (A) and Tizate thermal areas (B) is consistent with results from a previous soil CO_2 survey at San Jacinto (Ostapenko & Romero, 1995), and with the obvious thermal activity in those areas (Figure 9). Figure 9 also shows that the SJ9 and SJ10 faults (C) both have several points along their length with CO_2 flux anomalies and that the Los Tablones and La Joya faults (D) are coincident with CO_2 flux anomalies.

The Los Tablones fault was transected numerous times during the CO_2 flux survey. Moderate to strong CO_2 flux anomalies were found at the intersection of the Los Tablones fault in the majority of the transects (Figure 9). This suggests that permeability extends over considerable distance (~4 km) along the fault.

The Los Tablones fault hosts a broad area of moderate to strong anomalous CO_2 flux midway along its length. It is possible that this area is the manifestation of the intersection of the Los Tablones fault with the EW striking El Porvenir and La Cruz faults. Alternatively, it could relate to the more northerly strike of this section of the Los Tablones Fault here, and hence more extensional movement relative to the predominant NNE striking sections.

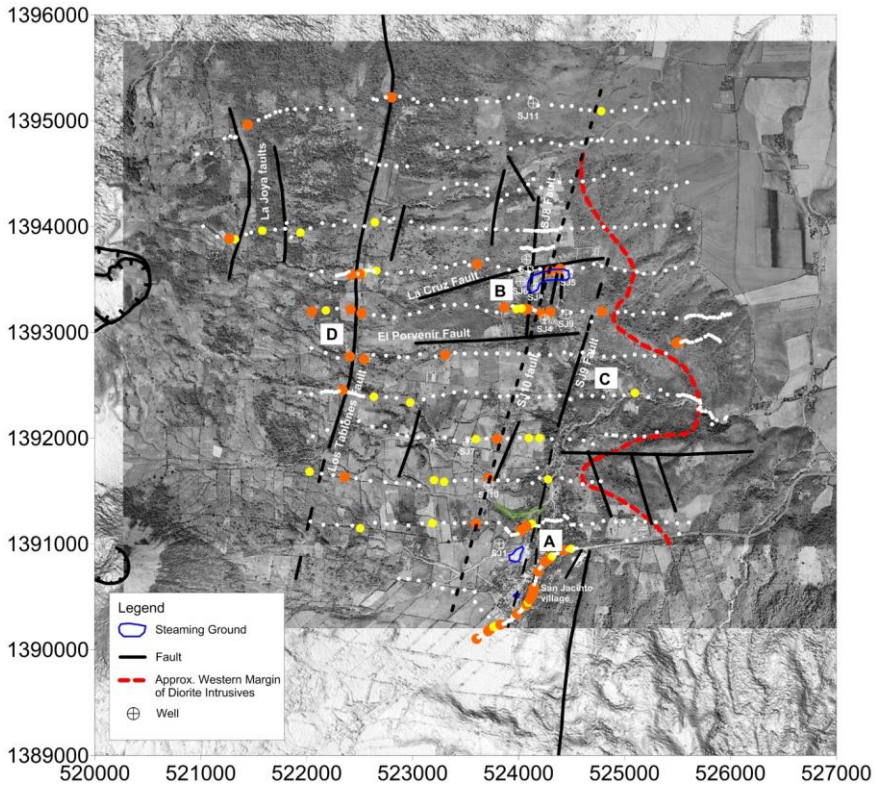

Figure 9: Soil CO_2 flux survey results. Small white dots are weak anomalies and background flux (≤ 80 g•m^{-2}•d^{-1}), yellow dots are moderate anomalies (80 – 100 g•m^{-2}•d^{-1}), and orange dots are strong anomalies (>100 g• m^{-2}•d^{-1}) (Harvey et al, 2011).

4. CONCLUSIONS

Our study has demonstrated a low cost approach to the production of georeferenced DSMs and orthophotos from aerial images captured by UAV. The ground resolution and position error of our DSM and orthophoto is comparable to commercially-produced LiDAR and aerial imagery obtained from manned aircraft.

High quality DSM/DEMs and orthophotos are useful in all phases of geothermal exploration and development including geological, geochemical and geophysical surveys, environmental baseline studies, geotechnical studies, civil works, steam field design, plant design and construction. As shown by the example DEM from the San Jacinto-Tizate survey (Figure 3), presumed fault locations can be identified and mapped.

We have also demonstrated the advantages of soil CO_2 flux surveys as a powerful and relatively inexpensive geothermal prospecting tool:

- Confirmation of the location and permeability of suspected faults
- Identification of the more permeable parts of major structures
- Identification of the existence of a geothermal system where thermal features are lacking
- Confirmation of the lateral extent of a geothermal system
- Estimation of total heat and fluid flow through permeable zones

Measurement of CO_2 flux in geothermal prospects has proven to be a useful technique for the exploration geologist/geochemist during the early stages of geothermal exploration. The technique is relatively low cost (requires a single operator carrying a small back pack), and provides results in real time allowing for dynamic adaptation of the survey design in response to results.

The combination of DSM mapping by UAVs, geological evaluation of structural features, and focused soil CO_2 flux surveys is particularly well suited for geothermal prospects in the East African Rift due to the arid climate, lack of vegetation, and remoteness.

REFERENCES

Bond-Lamberty, B.P. & Thomson, A.M. (2010). A Global Database of Soil Respiration Data, Version 1.0. Data set. Available on-line [http://daac.ornl.gov] from Oak Ridge National Laboratory Distributed Active Archive Center, Oak Ridge, Tennessee, U.S.A.

Chiodini, G., Cioni, R., Guidi, M., Raco, B., & Marini, L. (1998). Soil CO_2 flux measurements in volcanic and geothermal areas. *Applied Geochemistry, 13*(5), 543-552.

Fonstad, M. A., Dietrich, J. T., Courville, B. C., Jensen, J. L. & Carbonneau, P. E. (2013). Topographic structure from motion: a new development in photogrammetric measurement. *Earth Surf. Process. Landforms*, 38: 421–430. doi: 10.1002/esp.3366.

Fridriksson, T., B. R. Kristjánsson, H. Ármannsson, E. Margrétardóttir, S. Ólafsdóttir, & G. Chiodini (2006). CO_2 emissions and heat flow through soil, fumaroles, and steam heated mud pools at the Reykjanes geothermal area, SW Iceland, *Appl. Geochem., 21*, 1551-1569.

Harvey, M. C. & Alexander, K.B. (2011). Soil CO_2 flux surveys for geothermal exploration; lessons learned. *Geoscience Society of New Zealand Miscellaneous Publication* 129: 123

Harvey, M.C., White, P.J., MacKenzie, K.M. & Lovelock, B.G. (2011). Results from a soil CO_2 flux and shallow temperature survey at the San Jacinto-Tizate geothermal power project, Nicaragua. *New Zealand Geothermal Workshop 2011 Proceedings*, Auckland, New Zealand.

Harvey, M.C., Pearson, S., Alexander, K.B., Rowland, J. & White, P. (2014). Unmanned aerial vehicles (UAV) for cost effective aerial orthophotos and digital surface models (DSMs). *New Zealand Geothermal Workshop 2014 Proceedings (in press)*, Auckland, New Zealand.

Harvey, M.C. & Harvey, C.C. (2015). Soil CO_2 flux surveys: A review of the techniques in geothermal exploration. *Proceedings World Geothermal Congress 2015, Melbourne, Australia, 19-25 April 2015 (paper accepted)*.

Harwin S, Lucieer A. (2012). Assessing the accuracy of georeferenced point clouds produced via multi-view stereopsis from unmanned aerial vehicle (UAV) imagery. *Remote Sensing*; 4(6):1573-1599.

Lejot, J., Delacourt, C., Piégay, H., Fournier, T., Trémélo, M. L., & Allemand, P. (2007). Very high spatial resolution imagery for channel bathymetry and topography from an unmanned mapping controlled platform. *Earth Surface Processes and Landforms*, 32(11), 1705-1725.

Li, Z., Zhu, C., & Gold, C. (2010). Digital terrain modeling: principles and methodology. CRC press.

Priestnall, G., Jaafar, J., & Duncan, A. (2000). Extracting urban features from LiDAR digital surface models. *Computers, Environment and Urban Systems*, 24(2), 65-78.

Sinclair, A. J. (1974). Selection of threshold values in geochemical data using probability graphs, *J. Geochem. Explor*., 3, 129–149.

Van der Meer, F., Hecker, C., van Ruitenbeek, F., van der Werff, H., de Wijkerslooth, C., & Wechsler, C. (2014). Geologic remote sensing for geothermal exploration: A review. *International Journal of Applied Earth Observation and Geoinformation*, 33, 255-269.